Localization-Delocalization Transition of Indirect Excitons in Lateral Electrostatic Lattices

M. Remeika, J. C. Graves, A. T. Hammack, A. D. Meyertholen, M. M. Fogler, and L. V. Butov

Department of Physics, University of California at San Diego, La Jolla, California 92093-0319, USA

M. Hanson and A. C. Gossard

Materials Department, University of California at Santa Barbara, Santa Barbara, California 93106-5050, USA

We study transport of indirect excitons in GaAs/AlGaAs coupled quantum wells in linear lattices created by laterally modulated gate voltage. The localization-delocalization transition for transport across the lattice was observed with reducing lattice amplitude or increasing exciton density. The exciton interaction energy at the transition is close to the lattice amplitude. These results are consistent with the model, which attributes the localization-delocalization transition to the interaction-induced percolation of the exciton gas through the external potential. We also discuss applications of the lattice potentials for estimating the strength of disorder and exciton interaction.

Transport of particles in periodic potentials is a basic problem, which concerns a variety of systems extending from condensed-matter systems with electrons in ionic lattices to engineered systems such as photons in photonic crystals and cold atoms in optical lattices. The particle localization and localization-delocalization transition (LDT) are perhaps the most interesting transport phenomena. Particular cases of the latter—the metal-insulator and superfluid-insulator transitions—have been extensively studied for electrons, photons, and cold atoms in lattices [1–6].

Both particle and lattice parameters can be controlled for cold atoms in lattices. This has been intensively used for the exploration of condensed-matter physics in a system of cold atoms in lattices [3–6]. Here we study excitons in electrostatic lattices created by a gate voltage. As for cold atoms in lattices, in this system parameters of both the lattice, e.g., the lattice amplitude, and the particles, e.g., the exciton density, can be controlled. However, parameters of excitons differ from the atomic ones by orders of magnitude. Therefore, exciton studies can give complementary insights into this exciting field.

An indirect exciton in coupled quantum wells (CQWs) is a bound state of an electron and a hole in separate wells [Fig. 1(a)]. Lifetimes of indirect excitons exceed those of regular excitons by orders of magnitude, and they can travel over large distances before recombination [7–12]. Also, due to their long lifetime, these bosonic particles can cool to temperatures well below the quantum degeneracy temperature $T_{dB} = 2\pi\hbar^2 n/(mgk_B)$ [13]. (In the studied CQW, excitons have the mass $m = 0.22m_0$, spin degeneracy $g = 4$, and $T_{dB} \approx 3$ K for the density per spin $n/g = 10^{10}$ cm^{-2}.) Furthermore, indirect excitons in CQW have a dipole moment ed, where d is close to the distance between the QW centers. This allows imposing external potentials $E(x, y) = edF_z(x, y) \propto V(x, y)$ for excitons using a laterally modulated gate voltage $V(x, y)$, which creates a trans-

verse electric field $F_z(x, y)$ [7,12,14–20]. These properties of indirect excitons distinguish them for studying transport of cold interacting particles in tunable lattices from regular excitons with $d = 0$. Regular excitons cannot travel far and cannot cool down to low temperatures due to their short lifetimes and also interact only weakly and are controlled less effectively by applied voltage due to the absence of a
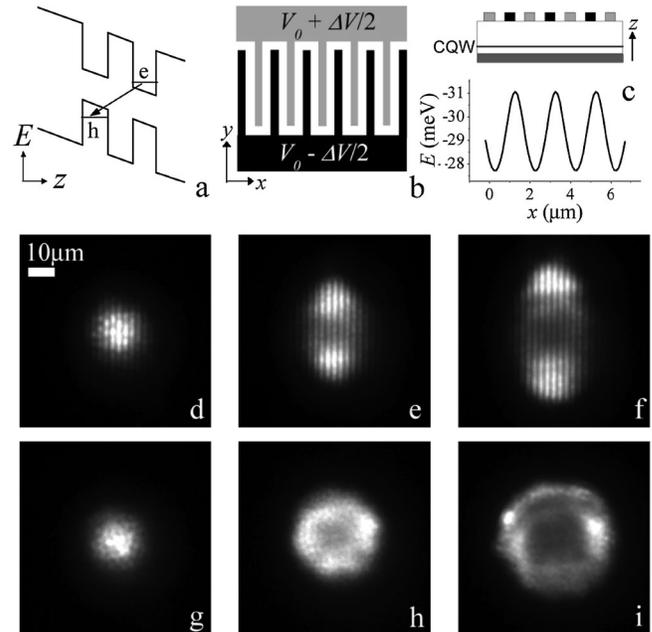

FIG. 1. (a) Energy band diagram of the CQW. (b), (c) Schematic electrode pattern. The applied base voltage V_0 realizes the indirect regime while the voltage modulation ΔV controls the lattice amplitude. Calculated lattice potential for indirect excitons for $\Delta V = 1$ V is shown in (c). PL images of indirect excitons for lattice amplitude (g)–(i) $\Delta V = 0$ and (d)–(f) $\Delta V = 1.2$ V for excitation powers (d),(g) $P = 0.2$, (e), (h) 3.7, and (f),(i) 12 μW. $T = 1.6$ K, $\lambda_{ex} = 633$ nm, and $V_0 = 3$ V for the data.

built-in dipole moment. Transport in lattices is an addition to a wide range of problems where indirect excitons are explored, including pattern formation, coherence, and condensation (see [21] and references therein), transport, and optoelectronics [7–12,14–20].

The lattice potential for indirect excitons $E(x)$ was created by interdigitated gates. Base voltage $V_0 = 3$ V realized the indirect regime where indirect excitons are lower in energy than direct excitons, while voltage modulation ΔV controlled the lattice amplitude [Figs. 1(b) and 1(c)]. Note that in-plane electric field F_r present near electrode edges can lead to exciton dissociation [14]. Therefore, the CQW layers in our structure were positioned closer to the homogeneous bottom electrode. This design suppresses F_r making the field-induced dissociation negligible [17]. An example of the calculated [17] (unscreened) $E(x)$ is shown in Fig. 1(c). Zero energy corresponds to zero voltage, and the 4 meV energy shift due to binding energy of the indirect exciton is not shown. The potential modulation is nearly sinusoidal: $E(x) = E_0 \cos^2(qx/2)$. Its amplitude is $E_0 = 3$ meV for $\Delta V = 1$ V and scales linearly with ΔV. The lattice period $2\pi/q = 2$ μm is determined by the electrode dimensions.

CQW structure was grown by molecular-beam epitaxy. An n^+-type GaAs layer with $n_{Si} = 10^{18}$ cm^{-3} serves as a homogeneous bottom electrode. Semitransparent top electrodes were fabricated by magnetron sputtering a 90 nm indium tin oxide layer. CQWs with 8 nm GaAs QWs separated by a 4 nm Al$_{0.33}$Ga$_{0.67}$As barrier were positioned 100 nm above the n^+-type GaAs layer within an undoped 1 μm thick Al$_{0.33}$Ga$_{0.67}$As layer. Excitons were photogenerated by a 633 nm HeNe or 786 nm Ti:sapphire laser focused to a spot ~10 μm in diameter in the center of the 150×150 μm lattice. The exciton density was controlled by the excitation power. Photoluminescence (PL) images of the exciton cloud were captured by a CCD with a bandpass filter 800 ± 5 nm covering the spectral range of the indirect excitons. The diffraction-limited spatial resolution was 1.5 μm [numerical aperture (NA) of 0.28]. The spectra were measured using a spectrometer with resolution 0.18 meV.

Figure 1 shows images of the exciton cloud at zero ($\Delta V = E_0 = 0$) and finite ($\Delta V = 1.2$ V, $E_0 = 3.7$ meV) lattice amplitude for different excitation powers P. At low P [Figs. 1(d) and 1(g)], the cloud profile essentially coincides with the laser excitation spot. This indicates that excitons do not travel beyond the excitation spot; i.e., they are localized. On the contrary, at high P [Figs. 1(e), 1(f), 1(h), and 1(i)], the excitons spread beyond the excitation spot indicating that they are delocalized. The LDT occurs both with and without the lattice.

The lattice potential also causes periodic modulations of PL characteristics. Figure 2 presents a PL image in energy-x coordinates in the delocalized regime. Both the integrated PL intensity $I(x)$ and the average PL energy $\hbar\omega(x)$ show a small modulation at the lattice period superimposed on a smoothly varying profile [Figs. 2(b)
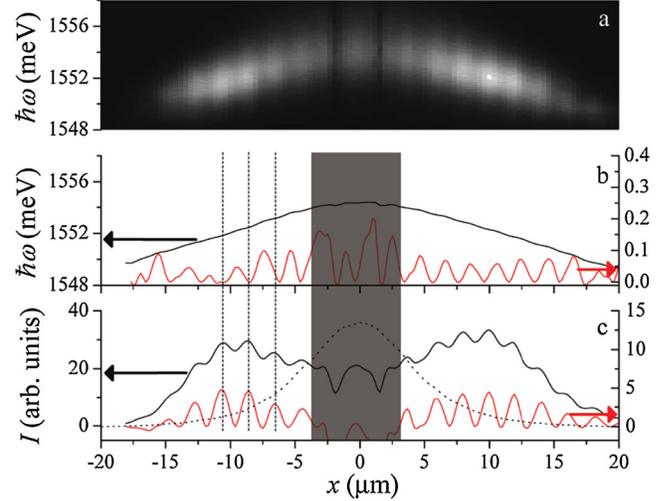

FIG. 2 (color online).   (a) The emission image in energy-x coordinates for the lattice with $\Delta V = 1.2$ V ($E_0 = 3.7$ meV). The image was measured at the center $y = 0$ of the exciton cloud and integrated over $\Delta y = 1.5$ μm. The corresponding (b) energy and (c) intensity profiles (black, left scale). The same profiles with subtracted smooth background are used to present the modulations in energy and intensity (red, right magnified scale). The energy minima correspond to intensity maxima. The PL linewidth does not exceed 2 meV that is characteristic of excitonic emission. The dotted line shows the profile of the laser excitation spot. The shaded area contains two deep intensity minima caused by a defect in the spectrometer slit. $T = 1.6$ K, $P = 35$ μW, $\lambda_{ex} = 633$ nm, and $V_0 = 3$ V for the data.

and 2(c)]. To demonstrate the modulations more clearly, we subtract the smooth component and plot the remainder on a magnified scale in Figs. 2(b) and 2(c). Minima in energy correspond to the maxima in intensity. We define the amplitude of energy modulation as the difference between adjacent maxima and minima $\delta\omega = \omega_{max} - \omega_{min}$. Figure 2 shows that $\hbar\delta\omega$ is much smaller than the lattice amplitude $E_0 = 3.7$ meV that is discussed below. No intensity or energy modulation was observed at $\Delta V = 0$. This indicates that the modulations in question are not due to the partial light absorption in the top electrodes.

The PL intensity has a maximum along a ring in the regime of delocalized excitons [Figs. 1(e), 1(f), 1(h), 1(i), and 2(c)]. This so-called inner ring was previously observed in PL patterns of indirect excitons without lattices [9]. It was explained in terms of exciton transport and cooling [9,11]. The inner ring effect persists in the lattice [Figs. 1(e), 1(f), and 2(c)].

The full width at half maximum of the exciton cloud in the x direction is plotted in Figs. 3(a) and 3(b). Initially, it is practically independent of P but then starts to grow as P increases. We define the excitation power at the transition P_{LDT} as the point where the extrapolation of this growth to small P becomes equal to the low-P constant. At the LDT, the exciton cloud starts to spread beyond the excitation spot, and the cloud extension changes from constant to increasing with P. Figure 3(a) shows that the transition is
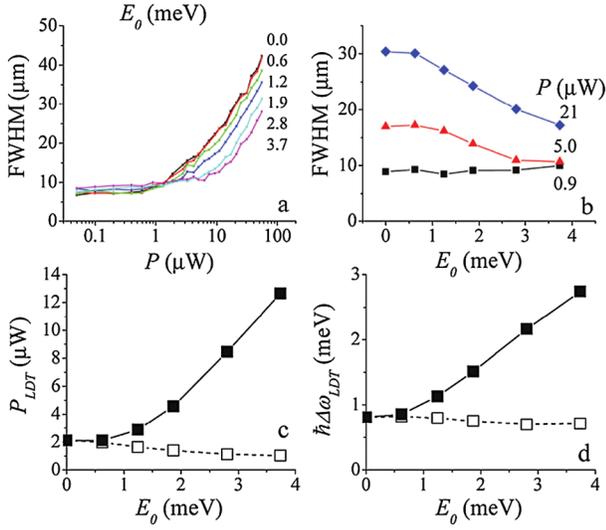
FIG. 3 (color online). The FWHM of the exciton cloud across the lattice (a) vs the excitation power P for lattice amplitudes $E_0 = 0$, 0.6, 1.2, 1.9, 2.8, and 3.7 meV ($\Delta V = 0$, 0.2, 0.4, 0.6, 0.9, and 1.2 V) and (b) vs E_0 for $P = 0.9$, 5, and 21 μW. (c) The excitation power at the transition from the localized to delocalized regime P_{LDT} as a function of E_0. (d) The interaction energy in the center of the exciton cloud at the transition from the localized to delocalized regime $\hbar\Delta\omega_{LDT}$ as a function of E_0. Filled (open) squares in (c),(d) present the data for the exciton transport across (along) the lattice. $T = 1.6$ K (see Ref. [31]), $\lambda_{ex} = 786$ nm, and $V_0 = 3$ V for the data.

smooth. This yields $P_{LDT} \approx 2$ μW for low lattice amplitudes $E_0 \lesssim 1$ meV. At higher E_0 the LDT for the x direction shifts to higher excitation powers with increasing lattice amplitude [Figs. 3(a) and 3(c)]. The LDT was also observed with reducing lattice amplitude; see the data for $P = 5$ μW [Fig. 3(b)]. Note that excitons remain localized at lower $P = 0.9$ μW and delocalized at higher $P = 21$ μW for all E_0 in Fig. 3(b).

The exciton transport along the y direction is only weakly affected by the lattice [Figs. 1(d)–1(i)]. The LDT for this direction shifts slightly to lower excitation powers with increasing E_0 [Fig. 3(c)].

The smooth component of the $\hbar\omega(x)$ also exhibits an interesting behavior. It increases with increasing exciton density, with both increasing P or reducing $|x|$. Let $\Delta\omega_{LDT}$ denote the difference between the value of ω at the lowest P and at the LDT at $x = 0$. Figure 3(d) presents the dependence of $\hbar\Delta\omega_{LDT}$ on E_0. We see that it is finite at $E_0 = 0$. At large E_0 we observe a remarkable relation

$$\hbar\Delta\omega_{LDT} \approx E_0, \qquad (1)$$

which is crucial to our interpretation of the mechanism of the LDT; see below.

Let us now discuss a simple model that attributes the observed LDT to the interaction-induced percolation of exciton gas through the total external potential $E_{tot}(\mathbf{r})$, which is the sum of the periodic lattice potential $E(x)$ and the random potential $E_{rand}(\mathbf{r})$ due to disorder. The latter

is an intrinsic feature of solid state materials. It forms mainly due to QW width and alloy fluctuations in the structure.

The idea is illustrated in Fig. 4 for the case of no disorder $E_{rand}(\mathbf{r}) \equiv 0$. If the local exciton density $n(x)$ is low, it is concentrated in the minima of the potential $E(x)$. The crests are nearly depleted. As a result, the exciton transport from one period of the lattice to the next through thermal activation or quantum tunneling is exponentially slow. As the average density increases and reaches a certain threshold—"percolation point"—the crests become populated, which permits a faster exciton transport, i.e., the observed delocalization. This scenario naturally leads to Eq. (1); see Fig. 4(b), where the middle curve corresponds to the percolation point. It also explains why P_{LDT} increases as E_0 goes up; see Fig. 3(d).

Adding disorder does not modify this picture greatly as long as E_0 remains larger than the characteristic amplitude of E_{rand}. Otherwise, the percolation is determined by the random potential [22,23], so that the dependence of P_{LDT} and $\Delta\omega_{LDT}$ on E_0 saturates. The saturation point gives the estimate of E_{rand}. From Fig. 3(d), we find $E_{rand} \sim 0.8$ meV. This number is comparable to the PL linewidth at low densities, suggesting that the disorder is responsible for both of these energy scales.

For further estimates, we make the following simplifying assumptions: (i) $E_{rand} \equiv 0$, while $E(x)$ can be considered slowly varying; (ii) excitons reach a quasiequilibrium state with local chemical potential $\mu(x)$ and temperature $T(x)$, which are also slowly varying; (iii) exciton interaction is local [dipolar tails (see below) are neglected]. Under these assumptions, we obtain

$$\zeta(x) \equiv \mu(x) + E(x) \simeq \text{const}, \qquad (2)$$

$$n(x) \simeq \int_0^\infty \frac{g\nu_1 d\epsilon}{\exp\{[\epsilon + \text{Re}\Sigma(\epsilon, x) - \mu(x)]/k_B T(x)\} - 1}, \qquad (3)$$
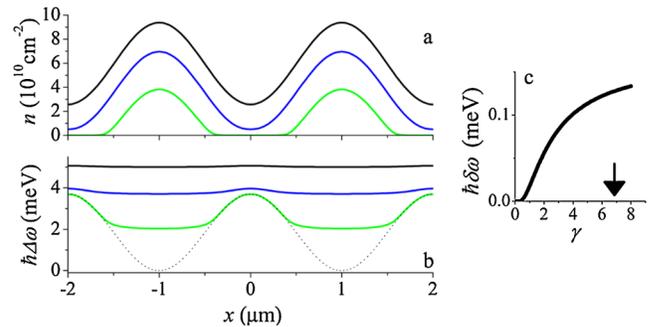

FIG. 4 (color online). (a) Exciton density for (top to bottom) $\zeta = 5$, 3.7, and 2.5 meV. The first of these corresponds to data at $x \sim 10$ μm in Fig. 2. $k_B T = 0.15$ meV, $E_0 = 3.7$ meV, and $\gamma = 2.3$ for all curves. (b) Lattice potential $E(x)$ and the PL energy shift $\hbar\Delta\omega(x)$ for the same set of parameters. (c) Modulation $\delta\omega = \omega_{max} - \omega_{min}$ of the PL energy as a function of the interaction strength γ. The experimental $\delta\omega$ corresponds to $\gamma \approx 2.3$. The value of γ predicted by the "capacitor" formula [26–28,30] is indicated by the arrow.

where ζ is the electrochemical potential, $\nu_1 = m/(2\pi\hbar^2)$ is the density of states per spin species, and $\Sigma(\epsilon)$ is the self-energy (in the uniform state of the same n).

To find the equation for the PL energy shift $\hbar\Delta\omega$, we take advantage of the smallness of Q, the range of in-plane momenta collected by our optical system. It is given by $Q \equiv 2\pi \times (\text{NA})/\lambda \approx (0.45~\mu\text{m})^{-1}$, which is indeed small. In this case $\hbar\Delta\omega(x) = \text{Re}\Sigma(0, x) + E(x)$.

To complete the system of equations, we need a formula for $\Sigma(\epsilon, x)$. This self-energy is due to the exciton interaction. At large r the interaction is known to be dominated by dipole repulsion $e^2d^2/(\kappa r^3)$. When excitons approach each other, the interaction potential becomes complicated. What appears to be certain is that for $d = 12$ nm in our experiment the exciton interaction remains strictly repulsive [24,25], and so $\text{Re}\Sigma(0)$ increases with density: $\text{Re}\Sigma(0) = tn$. The growth of $\text{Re}\Sigma(0)$ with n implies an increase of the PL energy $\hbar\omega$, which is observed experimentally. The calculation of function $t = t(n, T) > 0$ remains a challenging open problem [24,26–30]. For the following rough estimate, t is treated as a constant. We also assume that $\text{Re}\Sigma(\epsilon) \simeq \text{Re}\Sigma(0)$, which is reasonable for short-range interactions. Substituting $\Sigma = tn$ into Eq. (3), after some algebra we get

$$\exp\left(-\frac{n}{k_B T g \nu_1}\right) + \exp\left(\frac{\mu\nu_1 - \gamma n}{k_B T \nu_1}\right) = 1, \quad \mu = \zeta - E(x),$$

(4)

where the dimensionless parameter $\gamma = t\nu_1$ characterizes the strength of the interaction. Given ζ, T, and γ, Eq. (4) can be solved numerically for each $E(x)$. The results for $n(x)$ and $\Delta\omega(x)$ are shown in Figs. 4(a) and 4(b).

The exciton interaction results in screening of the lattice potential at points where local density is not small. Because of this screening, the amplitude of the PL energy modulation $\hbar\delta\omega$ is much smaller than E_0. Consider points $|x| \approx 10~\mu\text{m}$, on the inner ring. Here the exciton temperature is close to the sample temperature $T = 1.6$ K [11]. From Fig. 2(b), we see that $\hbar\delta\omega(x) \approx 0.07$ meV, more than an order of magnitude smaller than $E_0 = 3.7$ meV. Using the above equations, we calculated $\delta\omega$ as a function of the adjustable parameter γ; cf. Fig. 4(c). The experimental value of $\hbar\delta\omega$ gives a rough estimate $\gamma \approx 2.3$. In comparison, the mean-field Hartree approximation [26–28,30] yields the so-called "plate capacitor" formula $\gamma_{\text{cap}} = (2d/a_e)(m/m_e) \approx 7$, where $a_e = 10$ nm is the electron Bohr radius; see Fig. 4. The reduction of the interaction constant compared to the γ_{cap} can be due to correlation effects [24,29]. A systematic analysis of γ remains a problem for future research.

In summary, the localization-delocalization transition for exciton transport across a linear lattice was observed with reducing lattice amplitude or increasing exciton density. The exciton interaction energy at the transition is close to the lattice amplitude. These results were discussed in terms of the interaction-induced percolation of the exciton gas through the external potential. Applications of the lattice potentials for estimating the strength of disorder and exciton interaction were also discussed.

[1] P. A. Lee and T. V. Ramakrishnan, Rev. Mod. Phys. **57**, 287 (1985); D. Belitz and T. R. Kirkpatrick, Rev. Mod. Phys. **66**, 261 (1994).
[2] D. S. Wiersma *et al.*, Nature (London) **390**, 671 (1997).
[3] M. Greiner *et al.*, Nature (London) **415**, 39 (2002).
[4] C. D. Fertig *et al.*, Phys. Rev. Lett. **94**, 120403 (2005).
[5] J. K. Chin *et al.*, Nature (London) **443**, 961 (2006).
[6] G. Roati *et al.*, Nature (London) **453**, 895 (2008).
[7] M. Hagn, A. Zrenner, G. Böhm, and G. Weimann, Appl. Phys. Lett. **67**, 232 (1995).
[8] A. V. Larionov *et al.*, Sov. Phys. JETP **90**, 1093 (2000).
[9] L. V. Butov, A. C. Gossard, and D. S. Chemla, Nature (London) **418**, 751 (2002).
[10] Z. Vörös and K. West *et al.*, Phys. Rev. Lett. **94**, 226401 (2005).
[11] A. L. Ivanov *et al.*, Europhys. Lett. **73**, 920 (2006).
[12] A. Gartner *et al.*, Appl. Phys. Lett. **89**, 052108 (2006).
[13] L. V. Butov *et al.*, Phys. Rev. Lett. **86**, 5608 (2001).
[14] S. Zimmermann *et al.*, Phys. Rev. B **56**, 13 414 (1997).
[15] T. Huber *et al.*, Phys. Status Solidi A **166**, R5 (1998).
[16] J. Krauß *et al.*, Appl. Phys. Lett. **85**, 5830 (2004).
[17] A. T. Hammack *et al.*, J. Appl. Phys. **99**, 066104 (2006).
[18] G. Chen *et al.*, Phys. Rev. B **74**, 045309 (2006).
[19] A. A. High *et al.*, Opt. Lett. **32**, 2466 (2007).
[20] A. A. High *et al.*, Science **321**, 229 (2008).
[21] S. Yang *et al.*, Phys. Rev. Lett. **97**, 187402 (2006).
[22] P. Lugan *et al.*, Phys. Rev. Lett. **98**, 170403 (2007); T. Nattermann and V. L. Pokrovsky, Phys. Rev. Lett. **100**, 060402 (2008); B. I. Shklovskii, Semiconductors **42**, 909 (2008).
[23] Y. P. Chen *et al.*, Phys. Rev. A **77**, 033632 (2008).
[24] C. Schindler and R. Zimmermann, Phys. Rev. B **78**, 045313 (2008).
[25] A. D. Meyertholen and M. M. Fogler, Phys. Rev. B **78**, 235307 (2008).
[26] D. Yoshioka and A. H. MacDonald, J. Phys. Soc. Jpn. **59**, 4211 (1990).
[27] X. Zhu, P. B. Littlewood, M. Hybertsen, and T. Rice, Phys. Rev. Lett. **74**, 1633 (1995).
[28] Yu. E. Lozovik and O. L. Berman, JETP Lett. **64**, 573 (1996).
[29] S. Ben-Tabou de-Leon and B. Laikhtman, Phys. Rev. B **63**, 125306 (2001).
[30] A. L. Ivanov, Europhys. Lett. **59**, 586 (2002).
[31] See EPAPS Document No. E-PRLTAO-102-019921. For more information on EPAPS, see http://www.aip.org/pubservs/epaps.html.